

---

# Learning from Multi-View Representation for Point-Cloud Pre-Training

---

Siming Yan<sup>1</sup>

Chen Song<sup>1</sup>

Youkang Kong<sup>2</sup>

Qixing Huang<sup>1</sup>

<sup>1</sup>The University of Texas at Austin

<sup>2</sup>Microsoft Research Asia

## Abstract

A critical problem in the pre-training of 3D point clouds is leveraging massive 2D data. A fundamental challenge is to address the 2D-3D domain gap. This paper proposes a novel approach to point-cloud pre-training that enables learning 3D representations by leveraging pre-trained 2D-based networks. In particular, it avoids overfitting to 2D representations and potentially discarding critical 3D features for 3D recognition tasks. The key to our approach is a novel multi-view representation, which learns a shared 3D feature volume consistent with deep features extracted from multiple 2D camera views. The 2D deep features are regularized using pre-trained 2D networks through the 2D knowledge transfer loss. To prevent the resulting 3D feature representations from discarding 3D signals, we introduce the multi-view consistency loss that forces the projected 2D feature representations to capture pixel-wise correspondences across different views. Such correspondences induce 3D geometry and effectively retain 3D features in the projected 2D features. Experimental results demonstrate that our pre-trained model can be successfully transferred to various downstream tasks, including 3D detection and semantic segmentation, and achieve state-of-the-art performance.

## 1 Introduction

3D vision algorithms enable machines to perceive and interpret complex geometric structures, providing a deeper and more accurate understanding of the world than their 2D counterparts. The rapid development of commercial data acquisition devices [1] and point-based deep learning networks [2–4] has led to a growing research interest in models that can directly process 3D point clouds without voxelization. Remarkable success has been achieved in various applications, including but not limited to object detection [5–7], segmentation [8–10], and tracking [11–13].

Despite the significant advances in 3D point cloud processing, acquiring task-specific 3D annotations is a highly expensive and severely limited process due to the geometric complexity of the data. For example, ScanNet [14], a popular benchmark dataset for indoor 3D object detection, only contains 1,513 annotated scenes, which is only **0.01%** of the size of ImageNet [15], the benchmark dataset for 2D object detection, containing 14,197,122 labeled images. The shortage of data annotations highlights the need for adapting pre-training paradigms. Instead of training the deep network from randomly initialized weights, prior work suggests that pre-training the network on a relevant but different pre-task and later fine-tuning the weights using task-specific labels often leads to superior performance. In natural language processing and 2D vision, pre-trained models are the backbones of many exciting applications, such as real-time chatbots [16, 17] and graphic designers [18, 19]. However, pre-training on point clouds has yet demonstrated a universal performance improvement. From-scratch training remains a common practice in 3D vision.

Initial attempts towards 3D point-cloud pre-training primarily leverage contrastive learning [20], especially when the point clouds are collected from indoor scenes [21–25]. However, the broad

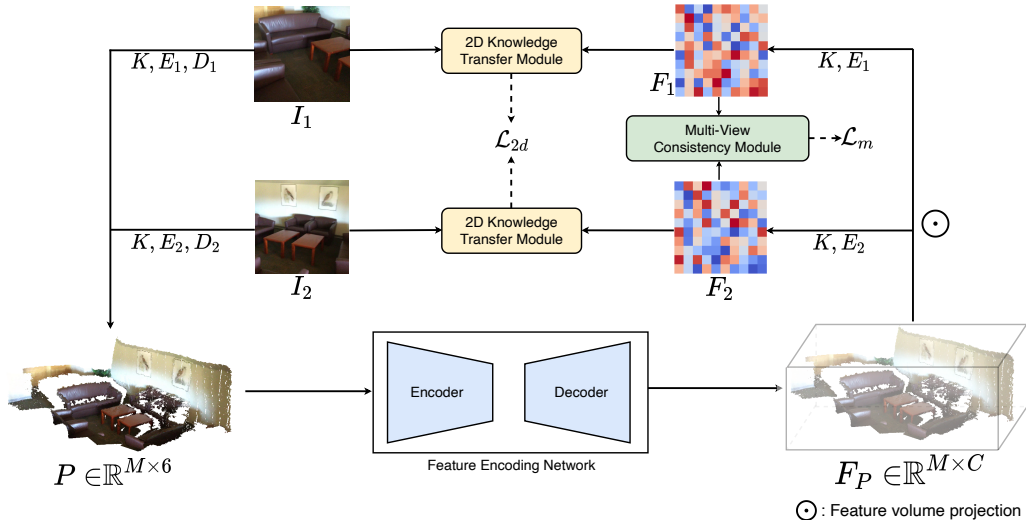


Figure 1: **Approach overview.** Please refer to Section 3 and Algorithm 1 for details.

application of contrastive learning-based pre-training techniques is impeded by the requirement of large batch sizes and the necessity to carefully define positive and negative pairs. In contrast to natural language processing and 2D vision, pre-training on 3D point clouds presents three unique challenges. First, the data is extremely scarce, even without annotations. Public 3D datasets are orders of magnitude smaller than 2D image datasets, potentially limiting their usefulness for pre-training. Besides, 3D point clouds are unstructured representations of complex geometries, creating a sharp contrast to 2D images, which are structured representations of much simpler geometries. In addition, the lack of data annotations necessitates 3D pre-training methods adhere to the self-supervised learning paradigm. Without strong supervision, pre-task design becomes particularly crucial in ensuring effective knowledge acquisition.

Figure 1 illustrates our novel approach to 3D pre-training, which is designed to address the aforementioned challenges. Our key idea is to leverage pre-trained 2D networks in the image domain to enhance the performance of 3D representation learning while bridging the 2D-3D domain gap. We begin by applying a 3D-based network to an input point cloud with  $M$  points, which generates a 3D feature volume represented by an  $M \times C$ -dimensional embedding, where  $C$  is the length of the per-point feature vectors. To compensate for data scarcity, we align the 3D feature volume with features predicted by a 2D encoder trained on hundreds of millions of images. To this end, we project the 3D feature volume into pixel embeddings and obtain an  $H \times W \times C$  image-like feature map in 2D. We then use pre-trained image encoders to extract hierarchical features from the corresponding RGB image and train a similarly structured encoder on the projected 2D map to enforce feature alignment. To ensure geometrical meaningfulness, we project the same 3D feature volume into multiple camera views and perform hierarchical feature alignment in each individual view. Our pipeline is generic enough to support all major 2D pre-trained models (e.g., CLIP [26], SAM [27], DINOv2 [28]). In our experiments, DINOv2 exhibits the best performance.

One issue with the approach described above is that the 3D feature learning may overfit to the pre-trained 2D networks. Consequently, it could potentially discard 3D features that are critical for 3D recognition but not well-captured during image-based 2D pre-training. To address this issue, we introduce an auxiliary pre-task to predict 2D multi-view pixel-wise correspondences from pairs of projected 2D feature maps. As such correspondences induce 3D depth information, the learned feature representations are forced to capture 3D signals.

Compared to existing approaches, our approach involves explicit 3D modeling in the feature space and leverages RGB images to enhance pre-training. RGB images are readily available in many 3D datasets, particularly those collected by RGB-D sensors in indoor settings [14]. However, their importance is often overlooked in prior work.

In summary, we make the following contributions:

- We formulate point-cloud pre-training as learning a multi-view consistent 3D feature volume.
- To compensate for data scarcity, we leverage pre-trained 2D image-based models to supervise 3D pre-training through perspective projection and hierarchical feature-based 2D knowledge transfer.
- To prevent overfitting to pre-trained 2D networks, we develop an auxiliary pre-task where the goal is to predict the multi-view pixel-wise correspondences from the 2D pixel embeddings. These embeddings are obtained by projecting the 3D feature volume into different camera views.
- We conduct extensive experiments to demonstrate the effectiveness of our approach in various downstream tasks, including 3D objection detection and semantic segmentation. Our approach achieves consistent improvements from baseline models.

## 2 Related work

**Point-based 3D recognition** The success of point-based deep neural networks [2–4] demonstrates the potential for machines to directly perceive point clouds. Existing research in point-based 3D vision can be categorized into three branches based on the data range: approaches that handle shape-level point clouds, algorithms that process indoor scene-level point clouds, and methods that deal with large-scale outdoor point clouds. Important applications include shape-level classification [29, 30] and part segmentation [31], as well as indoor scene-level detection [14, 32] and segmentation [33]. In the outdoor setting, a crucial task is critical object detection, where an autonomous driving system is trained to locate surrounding vehicles, pedestrians, and cyclists [34–41]. This paper focuses on indoor scenes, allowing downstream detection and segmentation tasks to benefit from the initial model weights pre-trained on the novel pre-task introduced in Section 3.

**Point-based pre-training** Point-based pre-training refers to the practice of *pre-training* the point-based prediction network on one or more *pre-tasks* before fine-tuning the weights on *downstream tasks*. The expectation is that the knowledge about pre-tasks will be transferred to downstream tasks, and the network can achieve better performance than random parameter initialization. We refer readers to [42] for a comprehensive survey, in which we highlight one important observation, stating that point-based pre-training “still lags far behind as compared with its counterparts”, and training from-scratch “is still the prevalent approach”. The challenges and opportunities call for innovations in point-based pre-training methods.

*Shape-level pre-training.* Self-reconstruction is a popular pre-task at the shape level, where the network encodes the given point cloud as representation vectors capable of being decoded back to the original input data [43, 44]. To increase the pre-task difficulty, it is common for self-reconstruction-based methods to randomly remove a certain percentage of the points from the input [45–49]. In addition to self-reconstruction, Rao et al. [50] develop a multi-task approach that unifies contrastive learning, normal estimation, and self-reconstruction into the same pipeline. There are also attempts to connect 3D pre-training to 2D [51–54]. For example, Dong et al. [53] utilize pre-trained 2D transformers as cross-modal teachers. Zhang et al. [54] leverage self-supervised pre-training and masked autoencoding to obtain high-quality 3D features from 2D pre-trained models. However, these methods focus on synthetic objects, leading to significant performance degradation in downstream tasks using real data from indoor scenes.

*Scene-level pre-training.* Existing scene-level pre-training methods focus on exploiting the contrastive learning paradigm. As the first pre-training method with demonstrated success at the scene level, PointContrast [21] defines the contrastive loss using pairs of 3D points across multiple views. RandomRoom [22] exploits synthetic datasets and defines the contrastive loss using pairs of CAD objects instead. Experimentally, RandomRoom affirms that synthetic shape-level pre-training is also beneficial to real-world scene-level downstream tasks. DepthContrast [24] simplifies PointContrast by proposing an effective pre-training method requiring only single-view depth scans. 4DContrast [25] further includes temporal dynamics in the contrastive formulation, where the pre-training data comprises sequences of synthetic scenes with objects in different locations. In contrast to these approaches, we focus on utilizing pre-trained 2D networks to boost the performance of 3D pre-training.

---

**Algorithm 1** General framework of MVNet

---

- 1: **Input:** RGB-D scan pairs with camera parameters  $S = \{(I_1^i, D_1^i), (I_2^i, D_2^i), K^i, E_1^i, E_2^i\}$ , feature encoding network  $\mathcal{F}_e$ , 2D knowledge transfer module  $\mathcal{F}_{2d}$ , multi-view consistency module  $\mathcal{F}_m$ .
  - 2: **Output:** Pre-trained weights of feature encoding network  $\mathcal{F}_e$
  - 3: **for**  $\{(I_1, D_1), (I_2, D_2), K, E_1, E_2\}$  **in** RGB-D scan pairs **do**
  - 4:     - Project  $(I_1, D_1), (I_2, D_2)$  into 3D point cloud  $P$  via camera parameters  $K, E_1, E_2$ .
  - 5:     - Extract per-point feature volume:  $F_P = \mathcal{F}_e(P)$ .
  - 6:     - Project the feature volume back onto the original views to generate 2D feature maps  $F_1, F_2$
  - 7:     - Employ 2D knowledge transfer module with square  $L_2$  loss:  $\mathcal{L}_{2d} = \mathcal{F}_{2d}(I_i, F_i)$
  - 8:     - Employ multi-view consistency module with the correspondence loss:  $\mathcal{L}_m = \mathcal{F}_m(F_1, F_2)$
  - 9:     - Compute the total loss  $\mathcal{L} = \mathcal{L}_{2d} + \lambda\mathcal{L}_m$ .
  - 10:    - Backprop: to update  $\mathcal{F}_e, \mathcal{F}_{2d}, \mathcal{F}_m$  with loss  $\mathcal{L}$ .
  - 11: **end for**
- 

### 3 Method

We present our pre-training approach pipeline, denoted as **MVNet** for brevity in the following sections. The entire process is illustrated in Figure 1 and Algorithm 1, and consists of several key steps. Given an RGB-D scan pair, we first project the 2D pixels into 3D point clouds using camera parameters. We then extract the point-cloud feature volumes using the feature encoding network (Section 3.1). Subsequently, we project the feature volume back onto the original views to generate 2D feature maps (Section 3.2). We design a 2D knowledge transfer module to learn knowledge from large-scale 2D pre-trained models (Section 3.3). Finally, we utilize the multi-view consistency module to ensure the agreement of different view features (Section 3.4). After pre-training, the pre-trained weights of the feature encoding network are transferred to downstream tasks for fine-tuning.

#### 3.1 Feature encoding network

Let  $(I_1, D_1)$  and  $(I_2, D_2)$  be two RGB-D scans from the same sequence, where  $I_1$  and  $I_2$  denote the RGB images, and  $D_1$  and  $D_2$  represent the depth maps. The camera intrinsic matrix is denoted as  $K$ , and the extrinsic matrices are denoted as  $E_1$  and  $E_2$ . By registering two different frames into the same world coordinate system, we map the RGB-D scans into a colored point cloud  $P \in \mathbb{R}^{M \times 6}$  of size  $M$ , with the first three channels representing coordinates and the remaining three channels representing RGB values.

Our approach leverages the Sparse Residual U-Net (SR-UNet) [4] as the backbone architecture. The point cloud  $P$  is initially voxelized based on its 3D coordinates, yielding a grid-based representation  $V \in \mathbb{R}^{M' \times 6}$ , where  $M' \ll M$  denotes the number of voxels. In our implementation, we set the voxel side length to 0.05 m. SR-UNet consists of an encoder and a decoder, which jointly generate  $C$ -dimensional per-voxel features  $F_V \in \mathbb{R}^{M' \times C}$ . We refer readers to the supplementary material for implementation details.

Next, we interpolate the per-voxel features  $F_V$  to obtain per-point features of the original point cloud, denoted as  $F_P \in \mathbb{R}^{M \times C}$ . This is achieved via the classical KNN algorithm based on point-to-point distances. The resulting  $F_P$  serves as our point-cloud feature volume, enabling further analysis and processing.

#### 3.2 Point-cloud feature volume projection

The key idea of MVNet is to learn 3D feature representations through 2D projections. This approach enables us to leverage large-scale pre-trained models in 2D and abundant 2D tasks for feature learning. To this end, we proceed to project the feature volume  $F_P$  back onto the original two views, generating 2D feature maps.

This projection operation uses the one-to-one mapping between each pixel in each input view and the corresponding 3D point in the concatenated 3D point cloud  $P$ . The results are two 2D feature maps  $F_1, F_2$ , each with dimensions  $H \times W \times C$ . In other words, the feature vector of each pixel takes that of the corresponding 3D point. Please refer to the supplementary material for more details.

### 3.3 2D knowledge transfer module

The first feature learning module of MVNet,  $\mathcal{F}_{2d}$ , aims to transfer knowledge from large-scale 2D pre-trained models. To this end, we consider each input RGB image  $I_i$  and the corresponding projected 2D feature map  $F_i$ . Our goal is to train  $F_i$  using a pre-trained 2D model  $f_p$  that takes  $I_i$  as input. The technical challenge is to address the difference between  $F_i$  and  $I_i$ . As illustrated in Figure 2, we introduce an additional network  $f_k$  that takes  $F_i$  as input.  $f_k$  shares the same network architecture as  $f_p$  except the first layer.

Let  $N$  be the number of layers in  $f_k$  and  $f_p$ . We define the training loss as

$$\mathcal{L}_{2d} = \sum_{i=3}^N \|B_i^{\text{pre-trained}} - B_i^{2D}\|_2^2 \quad (1)$$

where  $B_i^{\text{pre-trained}}$  denotes the output feature map of the  $i$ -th block in the pre-trained 2D model  $f_p$ , and  $B_i^{2D}$  denotes the output feature map of the  $i$ -th block in  $f_k$ . The objective of the 2D knowledge transfer process is to minimize  $\mathcal{L}_{2d}$ , thereby enabling  $f_k$  to learn the hierarchical features through knowledge transfer from the pre-trained 2D model. We add the loss starting from the third layer, which achieves the best performance in our implementation.

During training, the weights of the 2D pre-trained model  $f_p$  are unchanged, while  $f_k$  and the feature encoding network are jointly optimized. In our implementation, we select ViT-B [55] as the network backbone for both 2D neural network  $f_k$  and  $f_p$ , and we take the pre-trained weights of DINOv2 [28] for  $f_p$ . DINOv2 has been demonstrated to generate features with strong transferability. We refer readers to Section 4.3 for a detailed analysis.

### 3.4 Multi-view consistency module

The goal of the previous module is to leverage pre-trained 2D networks. However, the pre-trained 2D networks only contain feature representations that are primarily suitable for 2D tasks. Merely using this module does not prevent the 3D feature encoding network from discarding 3D features that are important for 3D recognition tasks. To address this issue, we introduce a novel multi-view consistency module  $\mathcal{F}_m$ , where the goal is to use the projected features  $F_1$  and  $F_2$  to predict dense correspondences between the two corresponding input images. Our motivation is that dense pixel-wise correspondences between calibrated images can recover 3D geometry. Therefore, enforcing ground-truth correspondences to be recoverable from  $F_1$  and  $F_2$  prevents the learned feature volume from discarding 3D features.

Our dense correspondence module adopts the architecture of COTR [56], which employs a transformer-based network to extract correspondences between two views. As depicted in Figure 3, we first use a backbone CNN  $\mathcal{C}$  to generate feature maps of size  $16 \times 16 \times 256$ . Next, we concatenate the two views side by side, forming a feature map  $F_c$  of size  $16 \times 32 \times 256$ . The context feature map  $F_c$  is fed into a transformer encoder  $\mathcal{T}_E$  and interpreted by a transformer decoder  $\mathcal{T}_D$ , along with the query point  $x$  from the first view  $I_1$ . Finally, we process the output of the transformer decoder with a fully connected layer  $\mathcal{D}$  to obtain our estimate for the corresponding point,  $x'$ , in the second view  $I_2$ :

$$x' = \mathcal{F}_m(x|F_1, F_2) = \mathcal{D}(\mathcal{T}_D(x, \mathcal{T}_E(\mathcal{C}(F_1) \oplus \mathcal{C}(F_2)))) \quad (2)$$

Following [56], we design the loss for correspondence error and cycle consistency:

$$\mathcal{L}_m = \|x^{gt} - x'\|_2^2 + \|x - \mathcal{F}_m(x'|F_1, F_2)\|_2^2 \quad (3)$$

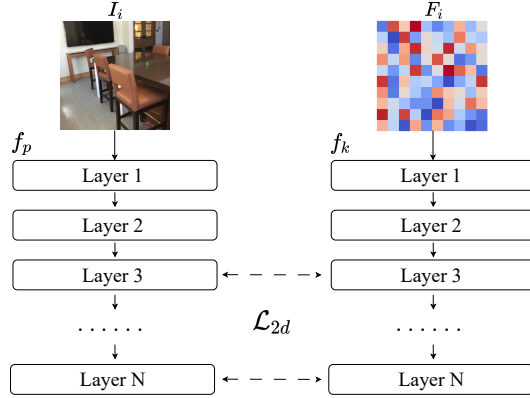


Figure 2: **Illustration of 2D knowledge transfer module.** During training,  $f_p$  remains frozen. For simplicity, we do not visualize the feature dimension of the feature map  $F_i$ .

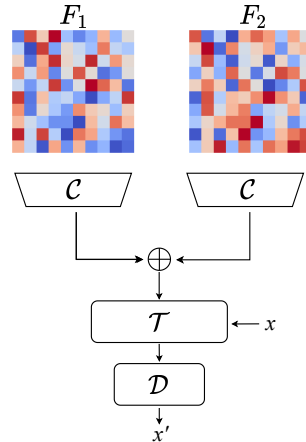


Figure 3: **Illustration of multi-view consistency module.**  $\oplus$  denotes side-by-side concatenation.

where  $x^{gt}$  denotes the ground truth corresponding point of  $x$  in the second view  $I_2$ .

Combing (1) and (3), the overall loss function is defined as:

$$\mathcal{L} = \mathcal{L}_{2d} + \lambda \mathcal{L}_m \quad (4)$$

where  $\lambda = 0.5$  is the trade-off parameter.

## 4 Experimental analysis

### 4.1 Pre-training setting

**Data preparation.** We choose ScanNet [14] as the pre-training dataset. ScanNet contains approximately 2.5 million RGB-D scans from 1,513 indoor scenes. Following Qi et al. [57], we extract 190K RGB-D scans (one every fifteen frames) from 1,200 video sequences in the training set. For each scan, we build the scan pair by taking it as the *first* scan ( $I_1, D_1$ ) and select five other frames with an overlap ratio between  $[0.4, 0.8]$  as the *second* scan ( $I_2, D_2$ ) candidates. We register the 2-view scans and map them to the world coordinate to generate a colored point cloud. The resulting point cloud serves as our pre-training input data.

**Network training.** Our pre-training model is implemented using PyTorch, employing the AdamW optimizer [58] with a weight decay of  $10^{-4}$ . For the feature encoding network, we use SR-UNet [21], comprising 21 convolution layers in the encoder and 13 convolution layers in the decoder, connected by skip connections. For the 2D knowledge transfer module, we use ViT-B [55] for feature extraction. In the multi-view consistency module, we take COTR [56] as the training network. The learning rate is set to  $10^{-3}$ . The model is trained for 200 epochs on eight 32GB Nvidia V100 GPUs, with 64 as the batch size.

### 4.2 Downstream tasks

The goal of pre-training is to learn features that can be transferred effectively to various downstream tasks. In the following experiments, we adopt the **supervised fine-tuning strategy**, which arguably provides the most practical evaluation of feature transferability. Specifically, the pre-trained weights serve as the initialization and are fine-tuned for the target downstream tasks.

#### 4.2.1 Semantic segmentation

**Datasets.** ScanNet [14] comprises 1,513 indoor scans. We use the original training and validation splits and report the mean Intersection over Union (IoU) on the validation split. S3DIS [33] consists of 272 rooms from 6 large areas. One area is chosen as the validation set, while the remaining areas are utilized for training. We report the mean IoU for Area-5 and the 6-fold cross-validation results.

**Network training.** We adopt SR-UNet [4] as the semantic segmentation architecture and add a head layer at the end of the feature encoding network for semantic class prediction. Although it is intuitive to transfer both the encoder and decoder pre-trained weights to the segmentation training, we observe that only transferring the encoder pre-trained weights results in better performance.

We fine-tune our model using the SGD+momentum optimizer with a batch size of 48, 10,000 iterations, and an initial learning rate of 0.01. We employ a polynomial-based learning rate scheduler with a power factor of 0.9. The same data augmentation techniques described by Chen et al. [25] are used, including hue/saturation modification and jittering, as well as scale variation ( $0.9 \times$  to  $1.1 \times$ ).

**Evaluation.** As demonstrated in Table 1, we achieve a +3.4 val mIoU improvement on ScanNet compared to training from scratch. To further validate the transferability, we evaluate our pre-trained model on the S3DIS dataset. Consistently, by fine-tuning with our pre-trained weights, we report +5.4/+4.7 mIoU improvements on the Area 5/6-Fold validation sets. On both datasets, we achieve the best performance compared to other self-supervised pre-training methods.

#### 4.2.2 3D object detection

**Datasets.** ScanNet [14] contains instance labels for 18 object categories, with 1,201 scans for training and 312 for validation. SUN RGB-D [32] comprises RGB-D images, with 5K images in the training set annotated with amodal, 3D-oriented bounding boxes for objects from 37 categories.

Method	S3DIS Area 5			S3DIS 6-Fold			ScanNet
	OA	mAcc	mIoU	OA	mAcc	mIoU	mIoU
PointNet [2]	53.5	49.0	41.1	78.5	66.2	47.6	-
PointCNN [59]	85.9	63.9	57.3	88.1	75.6	65.4	45.8
SPGraph [60]	86.4	66.5	58.0	85.5	73.0	62.1	-
PointWeb [61]	87.0	66.6	60.3	87.3	76.2	66.7	-
MinkowskiNet [4]	-	71.7	65.4	-	-	-	67.9
PointTransformer [10]	90.8	76.5	70.4	90.2	81.9	73.5	70.6
PointNeXt [8]	90.7	-	70.8	90.3	-	74.9	71.5
Stratified Trans [62]	91.5	78.1	72.0	-	-	-	74.3
PointMetaBase [63]	91.4	-	72.0	91.3	-	77.0	72.8
SR-UNet [21]	89.1	75.5	68.2	90.2	82.1	73.6	72.2
Jigsaw [64]	82.8	-	52.1	84.4	-	56.6	-
OcCo [65]	85.9	-	55.4	85.1	-	58.5	-
STRL [66]	-	-	-	84.2	-	57.1	-
PointContrast [21]	-	77.0	70.9	-	-	-	74.1
DepthContrast [24]	-	-	70.6	-	-	-	71.2
SceneContext [67]	-	-	72.2	-	-	-	73.8
MVNet	<b>91.6±0.1</b>	<b>79.3±0.2</b>	<b>73.3±0.3</b>	<b>91.7±0.1</b>	<b>86.2±0.1</b>	<b>78.1±0.2</b>	<b>75.2±0.4</b>
<i>Improvement</i>	<b>+2.6</b>	<b>+4.1</b>	<b>+5.4</b>	<b>+1.6</b>	<b>+4.2</b>	<b>+4.7</b>	<b>+3.4</b>

Table 1: **Semantic segmentation results on S3DIS (evaluation by 6-Fold or in Area 5) and ScanNet V2.** We show Overall Accuracy (OA), mean Accuracy (mAcc), and mean Intersection over Union (mIoU). Methods in the second section are self-supervised pre-training approaches. MVNet shows the average results of 3 runs.

Method	ScanNet		SUN RGB-D	
	mAP@0.25	mAP@0.5	mAP@0.25	mAP@0.5
Train from-scratch [57]	58.6	33.5	57.7	32.9
STRL [66]	59.5	38.4	58.2	35.0
RandomRooms [22]	61.3	36.2	59.2	35.4
PointContrast [21]	59.2	38.0	57.5	34.8
DepthContrast [24]	62.1	39.1	60.4	35.4
SceneContext [67]	-	39.3	-	36.4
4DContrast [25]	-	40.0	-	38.2
MVNet + VoteNet	<b>62.5±0.3</b>	<b>41.0±0.5</b>	<b>61.7±0.3</b>	<b>39.1±0.2</b>
<i>Improvement</i>	<b>+4.2</b>	<b>+8.0</b>	<b>+4.3</b>	<b>+6.4</b>

Table 2: **Comparison of 3D object detection results with self-supervised pre-training methods.** Following the previous pre-training approaches, we take VoteNet as the detection architecture and further fine-tune our pre-trained model on ScanNetV2 [14] and SUN-RGBD [32]. We show mean Average Precision (mAP) across all semantic classes with 3D IoU thresholds of 0.25 and 0.5.

**Network training.** We employ the encoder of the SR-UNet [4] as the detection encoder and transfer the pre-trained weights for network initialization. For the decoder design of 3D detection, we consider VoteNet [38] and CAGroup3D [7]. VoteNet is a classical 3D detection approach commonly used by existing self-supervised pre-training methods [21, 24, 22, 66]. However, VoteNet’s performance lags behind the state-of-the-art. Therefore, we also evaluate our approach on CAGroup3D, which offers a stronger decoder architecture and delivers state-of-the-art 3D detection performance.

During training, for the VoteNet setting, we fine-tune our model with the Adam optimizer (the batch size is 8, and the initial learning rate is 0.001). The learning rate is decreased by a factor of 10 after 80 and 120 epochs. For the CAGroup3D setting, we decrease the learning rate at 80 and 110 epochs.

**Evaluation.** As shown in Table 2, on ScanNet, our approach (MVNet) improves VoteNet by +4.2/+8.0 points on mAP@0.25 and mAP@0.5, outperforming other self-supervised pre-training approaches. Furthermore, as shown in Table 3, MVNet also enhances CAGroup3D by +0.7/+0.8 points on mAP@0.25 and mAP@0.5. On SUN RGB-D detection, MVNet exhibits consistent improvements. Specifically, MVNet achieves +4.3/+6.4 points on mAP@0.25 and mAP@0.5 under the VoteNet setting and +0.6/+1.2 points on mAP@0.25 and mAP@0.5 under the CAGroup3D setting.

Method	ScanNet		SUN RGB-D	
	mAP@0.25	mAP@0.5	mAP@0.25	mAP@0.5
VoteNet [57]	58.6	33.5	57.7	32.9
3D-MPA [68]	64.2	49.2	-	-
HGNet [69]	61.3	34.4	61.6	-
MLCVNet [70]	64.5	41.4	59.8	-
H3DNet [71]	67.2	48.1	60.1	39.0
BRNet [72]	66.1	50.9	61.1	43.7
3DETR [5]	65.0	47.0	59.1	32.7
VENet [73]	67.7	-	62.5	39.2
GroupFree [6]	69.1	52.8	63.0	45.2
RGBNet [74]	70.6	55.2	64.1	47.2
HyperDet3D [75]	70.9	57.2	63.5	47.3
FCAF3D [76]	71.5	57.3	64.2	48.9
CAGroup3D [7]	75.1	61.3	66.8	50.2
MVNet + CAGroup3D	<b>75.5±0.3</b>	<b>61.8±0.3</b>	<b>67.2±0.2</b>	<b>51.1±0.3</b>

Table 3: **Comparison of 3D object detection results with supervised methods.** We fine-tune our pre-trained model on ScanNetV2 [14] and SUN-RGBD [32] datasets using CAGroup3D [7].

### 4.3 Ablation study

We proceed to present an ablation study to justify our design choices. Due to the space constraint, we focus on the semantic segmentation results using the ScanNet dataset.

**Choice of 2D pre-trained models** As one of the most popular backbone architectures, ViT [55] has two variants: ViT-S and ViT-B. ViT-S (Small) contains 12 transformer blocks, each of which has 6 heads and 384 hidden dimensions. ViT-B (Base) contains 12 transformer blocks, each of which has 12 heads and 768 hidden dimensions. We also compare four different pre-training methods. As shown in Figure 4, ‘ViT-X’ represents pre-training the model by ImageNet-1K classification [15], ‘CLIP-X’ represents pre-training the model with the CLIP approach [26]. ‘SAM-X’ represents pre-training the model with the SAM approach [27]. ‘DINOv2-X’ represents pre-training the model with DINOv2 [28]. We observe that all the models show improvements compared with training from scratch (72.2 mIoU). Larger models (X-B) show consistent improvements compared with smaller models (X-S). DINOv2-B yields the best performance in terms of semantic segmentation accuracy on the ScanNet dataset. This demonstrates the advantage of leveraging DINOv2’s strong transferability properties in our method.

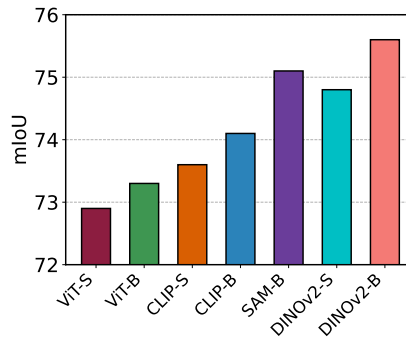


Figure 4: **Comparison of different 2D pre-trained models.**

**Loss design** Table 4a demonstrates the performance of our method with different loss configurations. We investigate the effectiveness of each loss component:  $\mathcal{L}_{2d}$  (2D knowledge transfer loss) and  $\mathcal{L}_m$  (multi-view consistency loss). The table shows that using either loss independently leads to an improvement in performance. However, combining both losses yields the best results, validating the importance of incorporating both 2D knowledge transfer and multi-view consistency in our approach.

**Masking ratio** Table 4b presents the performance of our method with varying masking ratios. The masking ratio determines the proportion of input data that is masked for each view during training. We find that a masking ratio of around 30% achieves the best performance, suggesting that maintaining a balance between visible and masked information is crucial for the model’s learning.

**View overlap ratio** In Table 4d, we examine the impact of the view overlap ratio on the performance of our method. The view overlap ratio refers to the percentage of a shared field of view between the two views used for multi-view consistency. It is important to note that in this experiment, we



(a) Loss design			(b) Masking ratio		(c) View number		(d) View overlap	
$\mathcal{L}_{2d}$	$\mathcal{L}_m$	ScanNet	Ratio (%)	ScanNet	Num	ScanNet	Overlap (%)	ScanNet
-	-	72.2	10	74.8	1	75.2	20	74.7
✓	-	74.8	20	75.2	2	75.2	40	75.1
-	✓	73.6	30	<b>75.6</b>	4	75.4	60	<b>75.2</b>
✓	✓	<b>75.6</b>	40	75.3	5	<b>75.6</b>	80	<b>75.2</b>

Table 4: **Ablation studies of our design choices.** We report the best val mIoU result on ScanNet. Please refer to Section 4.3 for a detailed analysis.

only use **one** candidate second view. We test ratios of 20%, 40%, 60%, and 80%. Compared to the results without the multi-view consistency loss (74.8 mIoU), our findings show that overlaps between 40% and 80% all result in improvements. However, when the overlap is too small, specifically at 20%, we fail to observe any improvement. We believe this is because when the overlap is insufficient, multi-view correspondences become too sparse, obtaining very limited 3D signals. As a result, our default setting selects views with overlaps in the range of [40%, 80%] as candidate second views, which ensures a balance between shared and unshared information for robust model performance.

**Number of views** As shown in Table 4c, we also investigate the impact of using different numbers of candidate second views in our multi-view consistency module. We experiment with 1 view, 2 views, 4 views, and 5 views. We find that incorporating more views leads to improved performance. Using 5 views shows the best performance. We did not experiment with more views as we observed that when the number of views exceeds 5, some candidates have a very small overlap with the first scan, which, as proven in the previous paragraph, can impede the learning of the multi-view consistency module.

**2D knowledge transfer loss** In this subsection, we investigate the optimal starting layer for adding the feature-based loss during the 2D knowledge transfer process. We explore the impact of incorporating the loss from different layers of the 2D neural network  $f_k$ .

As shown in Figure 5, our results reveal that adding the feature-based loss starting from the third layer yields the best performance in terms of semantic segmentation val mIoU on the ScanNet dataset. When adding the loss on the first and second layers, the model’s performance is negatively impacted. We believe this is because the inputs of the 2D pre-trained model and the 2D neural network differ. Forcefully adding the loss on the early layers may not be beneficial.

Furthermore, the performance drops when the loss is added starting from the fourth layer and beyond. This demonstrates that only regularizing the last few layers weakens the knowledge transferred from the pre-trained networks.

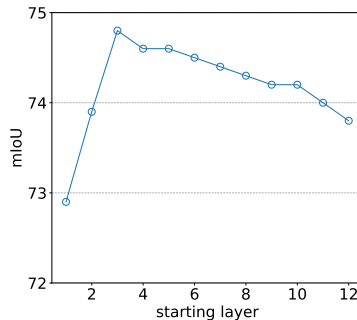


Figure 5: **Comparison of 2D knowledge transfer loss on different starting layers.**

## 5 Conclusion and limitation

In this paper, we present a novel approach to 3D point-cloud pre-training. Our approach leverages pre-trained 2D image-based encoders to supervise 3D pre-training through perspective projection and hierarchical feature-based 2D knowledge transfer. We also introduce a novel pre-task to enhance the geometric structure through correspondence prediction. Our experimental results demonstrate the effectiveness of our approach on various downstream tasks, achieving consistent improvements over baseline models.

Potential avenues for future work include exploring the performance of our approach with additional pre-training data, such as NYUv2 [77], and investigating the effect of increasing the size of the feature encoding network. Furthermore, we plan to extend our approach to outdoor settings and evaluate its effectiveness on larger-scale outdoor datasets. Overall, we believe that our work opens up new avenues for 3D point-cloud pre-training and provides a promising direction for future research.

## References

- [1] Morteza Daneshmand, Ahmed Helmi, Egils Avots, Fatemeh Noroozi, Fatih Alisinanoglu, Hasan Sait Arslan, Jelena Gorbova, Rain Eric Haamer, Cagri Ozcinar, and Gholamreza Anbarjafari. 3d scanning: A comprehensive survey. *arXiv preprint arXiv:1801.08863*, 2018.
- [2] Charles R Qi, Hao Su, Kaichun Mo, and Leonidas J Guibas. Pointnet: Deep learning on point sets for 3d classification and segmentation. In *Proceedings of the IEEE conference on computer vision and pattern recognition*, pages 652–660, 2017.
- [3] Charles Ruizhongtai Qi, Li Yi, Hao Su, and Leonidas J Guibas. Pointnet++: Deep hierarchical feature learning on point sets in a metric space. *Advances in neural information processing systems*, 30, 2017.
- [4] Christopher Choy, JunYoung Gwak, and Silvio Savarese. 4d spatio-temporal convnets: Minkowski convolutional neural networks. In *Proceedings of the IEEE/CVF conference on computer vision and pattern recognition*, pages 3075–3084, 2019.
- [5] Ishan Misra, Rohit Girdhar, and Armand Joulin. An end-to-end transformer model for 3d object detection. In *Proceedings of the IEEE/CVF International Conference on Computer Vision*, pages 2906–2917, 2021.
- [6] Ze Liu, Zheng Zhang, Yue Cao, Han Hu, and Xin Tong. Group-free 3d object detection via transformers. In *Proceedings of the IEEE/CVF International Conference on Computer Vision*, pages 2949–2958, 2021.
- [7] Haiyang Wang, Shaocong Dong, Shaoshuai Shi, Aoxue Li, Jianan Li, Zhenguo Li, Liwei Wang, et al. Cagroup3d: Class-aware grouping for 3d object detection on point clouds. *Advances in Neural Information Processing Systems*, 35:29975–29988, 2022.
- [8] Guocheng Qian, Yuchen Li, Houwen Peng, Jinjie Mai, Hasan Hammoud, Mohamed Elhoseiny, and Bernard Ghanem. Pointnext: Revisiting pointnet++ with improved training and scaling strategies. *Advances in Neural Information Processing Systems*, 35:23192–23204, 2022.
- [9] Liyao Tang, Yibing Zhan, Zhe Chen, Baosheng Yu, and Dacheng Tao. Contrastive boundary learning for point cloud segmentation. In *Proceedings of the IEEE/CVF Conference on Computer Vision and Pattern Recognition*, pages 8489–8499, 2022.
- [10] Hengshuang Zhao, Li Jiang, Jiaya Jia, Philip HS Torr, and Vladlen Koltun. Point transformer. In *Proceedings of the IEEE/CVF International Conference on Computer Vision*, pages 16259–16268, 2021.
- [11] Haozhe Qi, Chen Feng, Zhiguo Cao, Feng Zhao, and Yang Xiao. P2b: Point-to-box network for 3d object tracking in point clouds. In *Proceedings of the IEEE/CVF conference on computer vision and pattern recognition*, pages 6329–6338, 2020.
- [12] Chaoda Zheng, Xu Yan, Jiantao Gao, Weibing Zhao, Wei Zhang, Zhen Li, and Shuguang Cui. Box-aware feature enhancement for single object tracking on point clouds. In *Proceedings of the IEEE/CVF International Conference on Computer Vision*, pages 13199–13208, 2021.
- [13] Jiayao Shan, Sifan Zhou, Zheng Fang, and Yubo Cui. Ptt: Point-track-transformer module for 3d single object tracking in point clouds. In *2021 IEEE/RSJ International Conference on Intelligent Robots and Systems (IROS)*, pages 1310–1316. IEEE, 2021.
- [14] Angela Dai, Angel X Chang, Manolis Savva, Maciej Halber, Thomas Funkhouser, and Matthias Nießner. Scannet: Richly-annotated 3d reconstructions of indoor scenes. In *Proceedings of the IEEE conference on computer vision and pattern recognition*, pages 5828–5839, 2017.
- [15] Jia Deng, Wei Dong, Richard Socher, Li-Jia Li, Kai Li, and Li Fei-Fei. Imagenet: A large-scale hierarchical image database. In *2009 IEEE conference on computer vision and pattern recognition*, pages 248–255. Ieee, 2009.
- [16] Hugo Touvron, Thibaut Lavril, Gautier Izacard, Xavier Martinet, Marie-Anne Lachaux, Timothée Lacroix, Baptiste Rozière, Naman Goyal, Eric Hambro, Faisal Azhar, Aurelien Rodriguez, Armand Joulin, Edouard Grave, and Guillaume Lample. Llama: Open and efficient foundation language models. *arXiv preprint arXiv:2302.13971*, 2023.
- [17] OpenAI. Gpt-4 technical report, 2023.
- [18] Chenlin Meng, Yutong He, Yang Song, Jiaming Song, Jiajun Wu, Jun-Yan Zhu, and Stefano Ermon. Sdedit: Guided image synthesis and editing with stochastic differential equations. In *International Conference on Learning Representations*, 2021.

- [19] Tengfei Wang, Ting Zhang, Bo Zhang, Hao Ouyang, Dong Chen, Qifeng Chen, and Fang Wen. Pretraining is all you need for image-to-image translation. *arXiv preprint arXiv:2205.12952*, 2022.
- [20] Sumit Chopra, Raia Hadsell, and Yann LeCun. Learning a similarity metric discriminatively, with application to face verification. In *2005 IEEE Computer Society Conference on Computer Vision and Pattern Recognition (CVPR'05)*, volume 1, pages 539–546. IEEE, 2005.
- [21] Saining Xie, Jiatao Gu, Demi Guo, Charles R Qi, Leonidas Guibas, and Or Litany. Pointcontrast: Unsupervised pre-training for 3d point cloud understanding. In *European Conference on Computer Vision*, pages 574–591. Springer, 2020.
- [22] Yongming Rao, Benlin Liu, Yi Wei, Jiwen Lu, Cho-Jui Hsieh, and Jie Zhou. Randomrooms: unsupervised pre-training from synthetic shapes and randomized layouts for 3d object detection. In *Proceedings of the IEEE/CVF International Conference on Computer Vision*, pages 3283–3292, 2021.
- [23] Yueh-Cheng Liu, Yu-Kai Huang, Hung-Yueh Chiang, Hung-Ting Su, Zhe-Yu Liu, Chin-Tang Chen, Ching-Yu Tseng, and Winston H Hsu. Learning from 2d: Contrastive pixel-to-point knowledge transfer for 3d pretraining. *arXiv preprint arXiv:2104.04687*, 2021.
- [24] Zaiwei Zhang, Rohit Girdhar, Armand Joulin, and Ishan Misra. Self-supervised pretraining of 3d features on any point-cloud. *arXiv preprint arXiv:2101.02691*, 2021.
- [25] Yujin Chen, Matthias Nießner, and Angela Dai. 4dcontrast: Contrastive learning with dynamic correspondences for 3d scene understanding. In *Computer Vision—ECCV 2022: 17th European Conference, Tel Aviv, Israel, October 23–27, 2022, Proceedings, Part XXXII*, pages 543–560. Springer, 2022.
- [26] Alec Radford, Jong Wook Kim, Chris Hallacy, Aditya Ramesh, Gabriel Goh, Sandhini Agarwal, Girish Sastry, Amanda Askell, Pamela Mishkin, Jack Clark, et al. Learning transferable visual models from natural language supervision. In *International conference on machine learning*, pages 8748–8763. PMLR, 2021.
- [27] Alexander Kirillov, Eric Mintun, Nikhila Ravi, Hanzi Mao, Chloe Rolland, Laura Gustafson, Tete Xiao, Spencer Whitehead, Alexander C Berg, Wan-Yen Lo, et al. Segment anything. *arXiv preprint arXiv:2304.02643*, 2023.
- [28] Maxime Oquab, Timothée Darcet, Théo Moutakanni, Huy Vo, Marc Szafraniec, Vasil Khalidov, Pierre Fernandez, Daniel Haziza, Francisco Massa, Alaaeldin El-Nouby, et al. Dinov2: Learning robust visual features without supervision. *arXiv preprint arXiv:2304.07193*, 2023.
- [29] Zhirong Wu, Shuran Song, Aditya Khosla, Fisher Yu, Linguang Zhang, Xiaoou Tang, and Jianxiong Xiao. 3d shapenets: A deep representation for volumetric shapes. In *Proceedings of the IEEE conference on computer vision and pattern recognition*, pages 1912–1920, 2015.
- [30] Mikaela Angelina Uy, Quang-Hieu Pham, Binh-Son Hua, Thanh Nguyen, and Sai-Kit Yeung. Revisiting point cloud classification: A new benchmark dataset and classification model on real-world data. In *Proceedings of the IEEE/CVF international conference on computer vision*, pages 1588–1597, 2019.
- [31] Li Yi, Vladimir G. Kim, Duygu Ceylan, I-Chao Shen, Mengyan Yan, Hao Su, Cewu Lu, Qixing Huang, Alla Sheffer, and Leonidas Guibas. A scalable active framework for region annotation in 3d shape collections. *ACM Trans. Graph.*, 35(6), 2016.
- [32] Shuran Song, Samuel P Lichtenberg, and Jianxiong Xiao. Sun rgb-d: A rgb-d scene understanding benchmark suite. In *Proceedings of the IEEE conference on computer vision and pattern recognition*, pages 567–576, 2015.
- [33] I. Armeni, A. Sax, A. R. Zamir, and S. Savarese. Joint 2D-3D-Semantic Data for Indoor Scene Understanding. *ArXiv e-prints*, February 2017.
- [34] Shaoshuai Shi, Xiaogang Wang, and Hongsheng Li. Pointcnn: 3d object proposal generation and detection from point cloud. In *Proceedings of the IEEE/CVF Conference on Computer Vision and Pattern Recognition (CVPR)*, June 2019.
- [35] Zetong Yang, Yanan Sun, Shu Liu, and Jiaya Jia. 3dssd: Point-based 3d single stage object detector. In *Proceedings of the IEEE/CVF Conference on Computer Vision and Pattern Recognition (CVPR)*, June 2020.
- [36] Yifan Zhang, Qingyong Hu, Guoquan Xu, Yanxin Ma, Jianwei Wan, and Yulan Guo. Not all points are equal: Learning highly efficient point-based detectors for 3d lidar point clouds. In *Proceedings of the IEEE/CVF Conference on Computer Vision and Pattern Recognition (CVPR)*, pages 18953–18962, June 2022.

- [37] Charles R. Qi, Wei Liu, Chenxia Wu, Hao Su, and Leonidas J. Guibas. Frustum pointnets for 3d object detection from rgb-d data. In *Proceedings of the IEEE Conference on Computer Vision and Pattern Recognition (CVPR)*, June 2018.
- [38] Charles R. Qi, Or Litany, Kaiming He, and Leonidas J. Guibas. Deep hough voting for 3d object detection in point clouds. In *Proceedings of the IEEE/CVF International Conference on Computer Vision (ICCV)*, October 2019.
- [39] Weijing Shi and Raj Rajkumar. Point-gnn: Graph neural network for 3d object detection in a point cloud. In *IEEE/CVF Conference on Computer Vision and Pattern Recognition (CVPR)*, June 2020.
- [40] Zetong Yang, Yanan Sun, Shu Liu, Xiaoyong Shen, and Jiaya Jia. Std: Sparse-to-dense 3d object detector for point cloud. In *Proceedings of the IEEE/CVF International Conference on Computer Vision (ICCV)*, October 2019.
- [41] Haitao Yang, Zaiwei Zhang, Xiangru Huang, Min Bai, Chen Song, Bo Sun, Li Erran Li, and Qixing Huang. Lidar-based 3d object detection via hybrid 2d semantic scene generation. *arXiv preprint arXiv:2304.01519*, 2023.
- [42] Aoran Xiao, Jiaying Huang, Dayan Guan, Xiaoqin Zhang, Shijian Lu, and Ling Shao. Unsupervised point cloud representation learning with deep neural networks: A survey. *IEEE Transactions on Pattern Analysis and Machine Intelligence*, 2023.
- [43] Yaoqing Yang, Chen Feng, Yiru Shen, and Dong Tian. Foldingnet: Point cloud auto-encoder via deep grid deformation. In *Proceedings of the IEEE conference on computer vision and pattern recognition*, pages 206–215, 2018.
- [44] Siming Yan, Zhenpei Yang, Haoxiang Li, Li Guan, Hao Kang, Gang Hua, and Qixing Huang. Implicit autoencoder for point cloud self-supervised representation learning. *arXiv preprint arXiv:2201.00785*, 2022.
- [45] Hanchen Wang, Qi Liu, Xiangyu Yue, Joan Lasenby, and Matt J Kusner. Unsupervised point cloud pre-training via occlusion completion. In *Proceedings of the IEEE/CVF international conference on computer vision*, pages 9782–9792, 2021.
- [46] Yatian Pang, Wenxiao Wang, Francis EH Tay, Wei Liu, Yonghong Tian, and Li Yuan. Masked autoencoders for point cloud self-supervised learning. In *Computer Vision—ECCV 2022: 17th European Conference, Tel Aviv, Israel, October 23–27, 2022, Proceedings, Part II*, pages 604–621. Springer, 2022.
- [47] Renrui Zhang, Ziyu Guo, Peng Gao, Rongyao Fang, Bin Zhao, Dong Wang, Yu Qiao, and Hongsheng Li. Point-m2ae: multi-scale masked autoencoders for hierarchical point cloud pre-training. *arXiv preprint arXiv:2205.14401*, 2022.
- [48] Xumin Yu, Lulu Tang, Yongming Rao, Tiejun Huang, Jie Zhou, and Jiwen Lu. Point-bert: Pre-training 3d point cloud transformers with masked point modeling. In *Proceedings of the IEEE/CVF Conference on Computer Vision and Pattern Recognition*, pages 19313–19322, 2022.
- [49] Siming Yan, Yuqi Yang, Yuxiao Guo, Hao Pan, Peng-shuai Wang, Xin Tong, Yang Liu, and Qixing Huang. 3d feature prediction for masked-autoencoder-based point cloud pretraining. *arXiv preprint arXiv:2304.06911*, 2023.
- [50] Yongming Rao, Jiwen Lu, and Jie Zhou. Global-local bidirectional reasoning for unsupervised representation learning of 3d point clouds. In *Proceedings of the IEEE/CVF Conference on Computer Vision and Pattern Recognition*, pages 5376–5385, 2020.
- [51] Mohamed Afham, Isuru Dissanayake, Dinithi Dissanayake, Amaya Dharmasiri, Kanchana Thilakarathna, and Ranga Rodrigo. Crosspoint: Self-supervised cross-modal contrastive learning for 3d point cloud understanding. In *Proceedings of the IEEE/CVF Conference on Computer Vision and Pattern Recognition*, pages 9902–9912, 2022.
- [52] Chenfeng Xu, Shijia Yang, Tomer Galanti, Bichen Wu, Xiangyu Yue, Bohan Zhai, Wei Zhan, Peter Vajda, Kurt Keutzer, and Masayoshi Tomizuka. Image2point: 3d point-cloud understanding with 2d image pretrained models. *arXiv preprint arXiv:2106.04180*, 2021.
- [53] Runpei Dong, Zekun Qi, Linfeng Zhang, Junbo Zhang, Jianjian Sun, Zheng Ge, Li Yi, and Kaisheng Ma. Autoencoders as cross-modal teachers: Can pretrained 2d image transformers help 3d representation learning? *arXiv preprint arXiv:2212.08320*, 2022.

- [54] Renrui Zhang, Liuhui Wang, Yu Qiao, Peng Gao, and Hongsheng Li. Learning 3d representations from 2d pre-trained models via image-to-point masked autoencoders. *arXiv preprint arXiv:2212.06785*, 2022.
- [55] Alexey Dosovitskiy, Lucas Beyer, Alexander Kolesnikov, Dirk Weissenborn, Xiaohua Zhai, Thomas Unterthiner, Mostafa Dehghani, Matthias Minderer, Georg Heigold, Sylvain Gelly, et al. An image is worth 16x16 words: Transformers for image recognition at scale. *arXiv preprint arXiv:2010.11929*, 2020.
- [56] Wei Jiang, Eduard Trulls, Jan Hosang, Andrea Tagliasacchi, and Kwang Moo Yi. Cotr: Correspondence transformer for matching across images. In *Proceedings of the IEEE/CVF International Conference on Computer Vision*, pages 6207–6217, 2021.
- [57] Charles R Qi, Or Litany, Kaiming He, and Leonidas J Guibas. Deep hough voting for 3d object detection in point clouds. In *proceedings of the IEEE/CVF International Conference on Computer Vision*, pages 9277–9286, 2019.
- [58] Ilya Loshchilov and Frank Hutter. Decoupled weight decay regularization. *arXiv preprint arXiv:1711.05101*, 2017.
- [59] Yangyan Li, Rui Bu, Mingchao Sun, Wei Wu, Xinhan Di, and Baoquan Chen. Pointcnn: Convolution on x-transformed points. *Advances in neural information processing systems*, 31:820–830, 2018.
- [60] Loic Landrieu and Martin Simonovsky. Large-scale point cloud semantic segmentation with superpoint graphs. In *Proceedings of the IEEE conference on computer vision and pattern recognition*, pages 4558–4567, 2018.
- [61] Hengshuang Zhao, Li Jiang, Chi-Wing Fu, and Jiaya Jia. Pointweb: Enhancing local neighborhood features for point cloud processing. In *Proceedings of the IEEE/CVF conference on computer vision and pattern recognition*, pages 5565–5573, 2019.
- [62] Xin Lai, Jianhui Liu, Li Jiang, Liwei Wang, Hengshuang Zhao, Shu Liu, Xiaojuan Qi, and Jiaya Jia. Stratified transformer for 3d point cloud segmentation. In *Proceedings of the IEEE/CVF Conference on Computer Vision and Pattern Recognition*, pages 8500–8509, 2022.
- [63] Haojia Lin, Xiawu Zheng, Lijiang Li, Fei Chao, Shanshan Wang, Yan Wang, Yonghong Tian, and Rongrong Ji. Meta architecture for point cloud analysis. *arXiv preprint arXiv:2211.14462*, 2022.
- [64] Jonathan Sauder and Bjarne Sievers. Self-supervised deep learning on point clouds by reconstructing space. *arXiv preprint arXiv:1901.08396*, 2019.
- [65] Peng-Shuai Wang, Yu-Qi Yang, Qian-Fang Zou, Zhirong Wu, Yang Liu, and Xin Tong. Unsupervised 3d learning for shape analysis via multiresolution instance discrimination. *ACM Trans. Graphic*, 2020.
- [66] Siyuan Huang, Yichen Xie, Song-Chun Zhu, and Yixin Zhu. Spatio-temporal self-supervised representation learning for 3d point clouds. In *Proceedings of the IEEE/CVF International Conference on Computer Vision*, pages 6535–6545, 2021.
- [67] Ji Hou, Benjamin Graham, Matthias Nießner, and Saining Xie. Exploring data-efficient 3d scene understanding with contrastive scene contexts. In *Proceedings of the IEEE/CVF Conference on Computer Vision and Pattern Recognition*, pages 15587–15597, 2021.
- [68] Francis Engelmann, Martin Bokeloh, Alireza Fathi, Bastian Leibe, and Matthias Nießner. 3d-mpa: Multi-proposal aggregation for 3d semantic instance segmentation. In *Proceedings of the IEEE/CVF conference on computer vision and pattern recognition*, pages 9031–9040, 2020.
- [69] Jintai Chen, Biwen Lei, Qingyu Song, Haochao Ying, Danny Z Chen, and Jian Wu. A hierarchical graph network for 3d object detection on point clouds. In *Proceedings of the IEEE/CVF conference on computer vision and pattern recognition*, pages 392–401, 2020.
- [70] Qian Xie, Yu-Kun Lai, Jing Wu, Zhoutao Wang, Yiming Zhang, Kai Xu, and Jun Wang. Mlcvnet: Multi-level context votenet for 3d object detection. In *Proceedings of the IEEE/CVF conference on computer vision and pattern recognition*, pages 10447–10456, 2020.
- [71] Zaiwei Zhang, Bo Sun, Haitao Yang, and Qixing Huang. H3dnet: 3d object detection using hybrid geometric primitives. In *Computer Vision—ECCV 2020: 16th European Conference, Glasgow, UK, August 23–28, 2020, Proceedings, Part XII 16*, pages 311–329. Springer, 2020.
- [72] Bowen Cheng, Lu Sheng, Shaoshuai Shi, Ming Yang, and Dong Xu. Back-tracing representative points for voting-based 3d object detection in point clouds. In *Proceedings of the IEEE/CVF Conference on Computer Vision and Pattern Recognition*, pages 8963–8972, 2021.

- [73] Qian Xie, Yu-Kun Lai, Jing Wu, Zhoutao Wang, Dening Lu, Mingqiang Wei, and Jun Wang. Venet: Voting enhancement network for 3d object detection. In *Proceedings of the IEEE/CVF International Conference on Computer Vision*, pages 3712–3721, 2021.
- [74] Haiyang Wang, Shaoshuai Shi, Ze Yang, Rongyao Fang, Qi Qian, Hongsheng Li, Bernt Schiele, and Liwei Wang. Rbgnet: Ray-based grouping for 3d object detection. In *Proceedings of the IEEE/CVF Conference on Computer Vision and Pattern Recognition*, pages 1110–1119, 2022.
- [75] Yu Zheng, Yueqi Duan, Jiwen Lu, Jie Zhou, and Qi Tian. Hyperdet3d: Learning a scene-conditioned 3d object detector. In *Proceedings of the IEEE/CVF Conference on Computer Vision and Pattern Recognition*, pages 5585–5594, 2022.
- [76] Danila Rukhovich, Anna Vorontsova, and Anton Konushin. Fcaf3d: Fully convolutional anchor-free 3d object detection. *arXiv preprint arXiv:2112.00322*, 2021.
- [77] Camille Couprie, Clément Farabet, Laurent Najman, and Yann LeCun. Indoor semantic segmentation using depth information. *arXiv preprint arXiv:1301.3572*, 2013.